Self-Assembly

DOI: 10.1002/anie.201007098

DNA Block Copolymer Doing It All: From Selection to Self-Assembly of Semiconducting Carbon Nanotubes**

Minseok Kwak, Jia Gao, Deepak K. Prusty, Andrew J. Musser, Vladimir A. Markov, Nikolaos Tombros, Marc C. A. Stuart, Wesley R. Browne, Egbert J. Boekema, Gerrit ten Brinke, Harry T. Jonkman, Bart J. van Wees, Maria A. Loi, and Andreas Herrmann**

The selective and controlled manipulation of carbon nanotubes has long been a key objective for the integration of these superb quasi one-dimensional materials into real technologies to take advantage of their unique electronic, mechanical, thermal, and optical properties.[1] A particular focus of carbon nanotube research has been the solubilization of bundled nanostructures to obtain individual tubes. Such a process allows for easier characterization, fabrication, and incorporation of functionalities in solution. Techniques for this purpose range from covalent chemical functionalization of the nanotube sidewalls and termini, which alters the electronic structure and can impair the performance,[2] to sonication in solutions of hydrophobic, aromatic, or amphiphilic dispersing agents.[3] The latter method affords dispersions of SWNTs with minimal introduction of defects, and an additional purification process (i.e. density gradient ultracentrifugation) allows the isolation of SWNTs with narrow diameter distributions.[4] More advanced dispersing agents, such as poly(9,9-di-*n*-octylfluorenyl-2,7-diyl) (PFO) derivatives, even are able to selectively solubilize certain semiconducting nanotube species in a narrow diameter distribution that are of particular technological interest.[5]

More complex systems involving SWNTs are nanotube field-effect transistors (FETs), which since their first report[6] have see great advances.[7] Most fabrication methods, however, still involve locating and manipulation of individual SWNTs on a substrate, which is a laborious serial process.[8] A much more desirable production technique is the programmable, large scale positioning of semiconducting carbon nanotubes; this approach, however, is still the holy grail for carbon nanotube electronics.[9]

As one of the most powerful building blocks for self-assembled nanostructures,[10] DNA has the potential to play a major role in any such development. Although the selective dispersion of SWNTs with pristine DNA was realized,[11] the subsequent controlled assembly through hybridization with complementary DNA (cDNA) is unfeasible because of the unwrapping of DNA attached to the tube.[12] Other studies that combine DNA and SWNTs have entailed covalent bond formation between the two moieties[13] or the chemical modification of DNA wrapped around the nanotubes.[14] These examples, although very important, had only partial success in versatile functionalization and scalable device applications, mostly due to the limited conditions and yield of the fabrication process but also because of an abundance of metallic tubes in the sample.[15]

Herein we report a straightforward solution to many of the key concerns that face SWNT technology (nondestructive dispersion of individual nanotubes, enrichment of semiconducting species, and precise supramolecular addressability) by using amphiphilic DNA block copolymers (DBCs, Figure 1 a). DBCs are best known for multifunctional self-assembled micelles[16] and especially biomedical applications thereof,[17] but we demonstrate herein that they effectively and selectively disperse SWNTs and offer a platform for manipulation and precise positioning. To the best of our knowledge, this work represents the first combination of high semiconducting SWNT affinity and versatile nondestructive functionalizability in a single material (Figure 1 b). The DBC used throughout this study consists of PFO covalently connected to 22-mer single-stranded (ss) oligodeoxynucleotides (ODNs). The hydrophobic polymer segments interact with the SWNT sidewall, thus enabling the dispersion of particular semiconducting nanotube species through a very simple procedure, as characterized by a range of spectroscopic and microscopic techniques. This interaction leaves the DNA block free for facile hybridization with targets in solution and site-specific immobilization onto surfaces (Figure 1 c), hence allowing the bottom-up fabrication of electronic devices on extended surface areas in extremely high yields (98% working devices, Figure 1 d).

Terminally hydroxymethyl-functionalized PFO (M_w: 6000 g mol^{-1}) was synthesized in five steps starting from 9,9-

[*] M. Kwak, J. Gao, D. K. Prusty, A. J. Musser, V. A. Markov, Dr. N. Tombros, Prof. Dr. G. ten Brinke, H. T. Jonkman, Prof. Dr. B. J. van Wees, Prof. Dr. M. A. Loi, Prof. Dr. A. Herrmann
Zernike Institute for Advanced Materials, University of Groningen
Nijenborgh 4, 9747 AG Groningen (The Netherlands)
Fax: (+31) 363-4400
E-mail: m.a.loi@rug.nl
a.herrmann@rug.nl
Homepage: http://bit.ly/pcberug
Dr. M. C. A. Stuart, Prof. E. J. Boekema
Groningen Biomolecular Sciences and Biotechnology Institute
9747 AG Groningen (The Netherlands)
Dr. W. R. Browne
Stratingh Institute for Chemistry
9747 AG Groningen (The Netherlands)

[**] This work was supported by the EU (ERC starting grant, ECCell), the Netherlands organization for scientific research (NWO-Vici, Echo), the German research foundation (DFG), and the Zernike Institute for Advanced Materials. J.G. and M.A.L. were supported by Nanoscience-ERA and NaPhoD.

Supporting information for this article is available on the WWW under http://dx.doi.org/10.1002/anie.201007098.

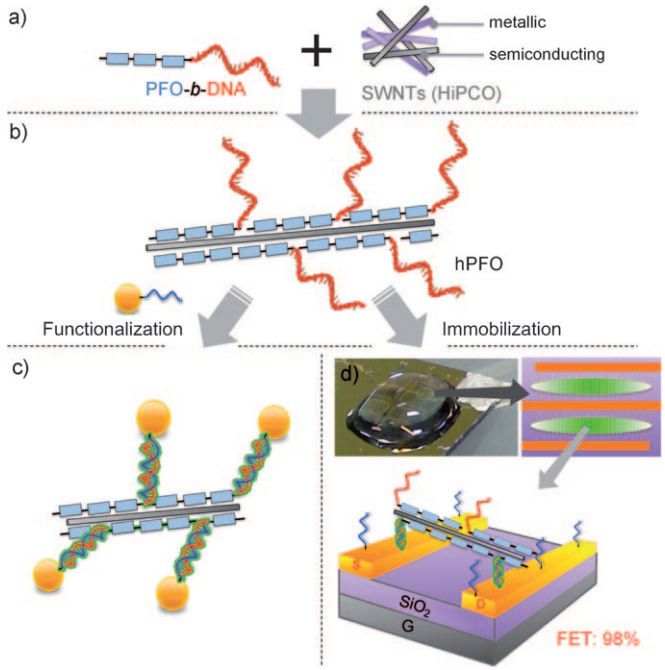

Figure 1. Representation of programmed functionalization of SWNTs and their sequence-specific assembly in nanoelectronic devices. a) Amphiphilic DBC structure for solubilization of SWNTs. b) Diameter-selective dispersion of SWNTs in aqueous media. c) Straightforward functionalization of the SWNT surface by hybridization. d) Unprecedented programmed assembly of SWNTs on surfaces or within nanoelectronic devices.

dioctyl-2,7-dibromofluorene, and the polymer was phosphitylated by using 2-cyanoethyl *N*,*N*-diisopropylchlorophosphoramidite.[18] As shown in Figure 2a, this activated polymer was attached to the 5′-end of a 22-mer ODN with the sequence 5′-CCT CGC TCT GCT AAT CCT GTT A-3′ by using standard solid-phase synthesis (see the Supporting Informatiom for detailed preparation and characterization). This sequence was selected because of its lack of a secondary structure and its compatibility with a wide range of experimental conditions.[16–17] It should be noted that this material represents the first DBC containing a conjugated polymer

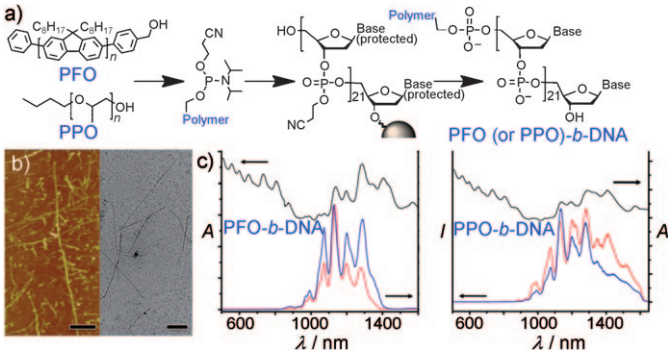

Figure 2. a) Synthesis of DBCs, PFO-*b*-DNA, and PPO-*b*-DNA. b) AFM topography of hPFO in contact mode (left) and uranyl acetate stained TEM micrograph of hPFO (right). Scale bars are 200 nm. c) Absorption (offset, black) and normalized PL spectra (blue: $\lambda_{ex} = 380$ nm, red: $\lambda_{ex} = 760$ nm) of hPFO and hPPO. The arrows indicate the corresponding axis of the spectrum.

segment that was produced in a single and fully automated process employing a DNA synthesizer. Owing to the utilization of phosphoramidite polymers, our fabrication process requires scarcely more effort than the synthesis of pristine ODNs.

To prepare carbon nanotube dispersions, an aqueous solution of the DNA block copolymer, PFO-*b*-DNA, was added to dry SWNTs, sonicated, and centrifuged to remove large bundles in the solution. After centrifugation, the gray supernatant was directly used for all characterization and application experiments without further purification. Other reference dispersions including a DBC with a hydrophobic block, poly(propylene oxide) (PPO),[19] were prepared under the same conditions unless otherwise noted.

To check the suitability of this procedure for the production of well-dispersed individual SWNTs, we performed tapping mode AFM measurements in air on DBC-dispersed high-pressure CO conversion (HiPCO) SWNTs (hPFO and hPPO) and DNA-dispersed HiPCO SWNTs (hDNA) using the same 22-mer sequence, all deposited on mica (see the Supporting Information). A representative height image of hPFO is shown in Figure 2b (left). All nanotubes observed had a height of less than 3 nm, thus suggesting individually dispersed SWNTs or small bundles (Figure S8 in the Supporting Information, larger aggregates could not be observed). This result was to be expected, as it is well known that DNA is especially efficient at keeping SWNTs stably separated because of electrostatic repulsion. This effect is reflected in the long-term stability of the dispersions, which stayed stable for at least three months without notable changes in optical characteristics. In contrast, nonionic triblock copolymer (Pluronic F127) and anionic surfactant (sodium dodecyl benzene sulfonate, SDBS) dispersion of SWNTs results in significant bundling as observed in TEM (Figure S11). The F127- and SDBS-dispersed nanotubes appear as large rope-like structures while single nanotubes are clearly resolved in hPFO (right in Figure 2b), hPPO, and hDNA (additional TEM images in Figures S9 and S10).

The DBC dispersions hPFO and hPPO were further investigated by UV/Vis/NIR absorption, NIR photoluminescence (PL), and Raman spectroscopy. The absorption spectra of both hPFO and hPPO showed the typical S1 and S2 bands of semiconducting species in wavelength ranges of 1000–1600 nm and 600–900 nm, respectively, which correspond to SWNTs with diameters in the range of 0.7–1.2 nm (Figure 2c). Furthermore, the absorption spectrum of hPFO showed markedly better-resolved structure[20] than that of hPPO, although they were prepared in the same way, thus indicating that PFO-*b*-DNA more effectively disperses individual SWNTs from bulk HiPCO. This result is presumably due to the strong interaction between PFO and SWNT sidewalls, as predicted by simulation results detailed below. The presence of strong characteristic near-infrared PL bands is direct evidence of individually dispersed SWNT species in hPFO and hPPO (Figure 2c).[3a]

Corresponding emission bands show the presence of primarily four nanotube species (indexed *n*, *m*) in hPFO, whereas hPPO contains more species under the same conditions.[21] Owing to the different local dielectric environ-

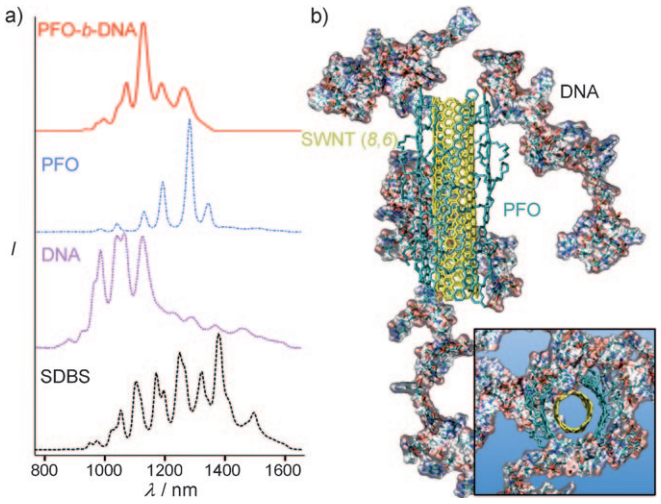

Figure 3. a) Normalized PL spectra of HiPCO dispersions with PFO-*b*-DNA (——), PFO (–•–•), DNA (••••), and SDBS (-----). Excitation: 760 nm. Note that the PFO dispersion is in toluene while others are in H_2O. b) Snapshots from MD simulation of a system with PFO-*b*-DNA and SWNT (*8,6*) in aqueous environment. Inset: axial view of hPFO.

ment, these bands are red-shifted by approximately 15 nm relative to the reported spectrum for an aqueous surfactant dispersion (Figure 3a).[22] For hPFO, the SWNT dispersion used most throughout this report, we assigned the most prominent PL peaks to the semiconducting (*7,5*), (*7,6*), (*8,6*), and (*8,7*) chiral indices (see Figure S13 for full assignment of hPFO). The (*8,7*) SWNT (marked in the inset of Figure S14) and other bands were observed in the radial breathing mode (RBM) range (200–280 cm^{-1}, $\lambda_{ex} = 785$ nm) of the Raman spectrum (Figure S14). As anticipated, low D/G band intensity ratios were observed for both dispersions, which is indicative of a low degree of structural defects and is a clear advantage of this separation technique.

Owing to the ability of both PFO and DNA to sort SWNTs, the remaining question is what the individual components of our new nucleic acid amphiphile, PFO-*b*-DNA, contribute to the dispersion. For this purpose we compare the PL spectra of hPFO and HiPCO SWNTs dispersed in PFO or DNA alone. From the spectra shown in Figure 3a, it is immediately apparent that PFO-*b*-DNA and both individual components are much more selective than a widely used aqueous dispersant, SDBS. The population in hPFO more closely resembles that of PFO-dispersed HiPCO in toluene[5a] (the gold standard for selective dispersion) than that of hDNA, particularly with regard to the diameter distribution. However, the population balance evident in hPFO is not quite identical to that of PFO in toluene—this difference can be partially attributed to the change of solvent, which is known to have a direct influence on selectivity.[23] We further propose that DNA wrapping contributes to this observation; the higher-than-expected population of small-diameter SWNTs ($\lambda_{em} < 1200$ nm) in hPFO may correlate with the most prominent bands of the hDNA PL spectrum. It might therefore be possible that in hPFO both the PFO and the DNA blocks contribute to SWNT dispersion.

In the cases where polymer wrapping is dominant, we claim that the hydrophobic PFO block of PFO-*b*-DNA envelops the SWNT surface while the DNA block extends from the nanotube and provides water solubility as well as steric and electrostatic stabilization. Such a preference for PFO wrapping could be due to the hydrophobic nature of the aromatic π systems of the conjugated polymer block and accordingly its greater binding to the nanotube surface than that of heterocyclic nucleobases. This explanation is supported by a molecular dynamics (MD) simulation of the hPFO system (Figure 3b, see the Supporting Information for simulation details). A short segment of (*8,6*) SWNT, denoted in Figure S13 and S14, was simulated in close proximity to four PFO-*b*-DNA molecules in two initial configurations, with either the PFO or DNA block being closer to the sidewall (Figure S15 and S16). In the former case, the complex was stable for the entire simulation (see movie S1 in the Supporting Information) with a PFO sidewall separation and conformation in consistency with other reported simulations (3.3 ± 0.1 Å).[5a,23] In the latter case, the interaction between the DNA block and the sidewall proved too weak and the binding was unstable, hence the entire molecule detached from the SWNT in less than one nanosecond. The interaction between the SWNT sidewall and PFO is therefore more favorable than the one between the sidewall and DNA. Indeed, in an additional simulation, in which the SWNT segment was initially surrounded by four PFO-*b*-DNA molecules in a stable configuration, these four DBCs shifted to accommodate the approach and complexation of the PFO block of a fifth DBC (Figure S17). The significance of these affinity results lies in the availability of the extended DNA strands for further manipulation by DNA hybridization.

To demonstrate the facile functionalization of this hPFO system, gold nanoparticles were chosen for convenient high-contrast visualization and were lined up along dispersed SWNTs by using DNA hybridization (Figure 1c). For this study, 5 nm diameter gold nanoparticles were conjugated to a single thiol-modified ODN (cDNA), with sequence complementarity to the 22-mer DNA block of PFO-*b*-DNA, and subsequently passivated with monothiolated poly(ethylene glycol) to prevent nonspecific adsorption (see the Supporting Information).[24] These DNA-labeled nanoparticles (Au-cDNA) were incubated with hPFO under hybridization conditions. The mixtures were then imaged by TEM without any further treatment or purification of the materials. The results were unambiguous, with a large population of dark spots arranged in proximity to linear fibrils (Figure 4a and b). Both hPFO and hPPO results showed similar alignment of gold nanoparticles along the SWNTs (Figure S19, S20, and S21); analogous structures were found in AFM in air and fluid (Figure S22).

In the same way that the fully addressable ss-DNA block allows supramolecular assembly onto nanotubes in solution, it also enables their specific deposition from solution onto cDNA-functionalized surfaces (see the Supporting Information). The simplest demonstration of this process was accomplished by an AFM study of hybridization to sparse thiol–ODN monolayers on gold. The SWNT coverage observed on the cDNA-functionalized surface was more than 4 times higher than that on a surface functionalized with noncomplementary DNA (Figure S23 and Table S5). While a

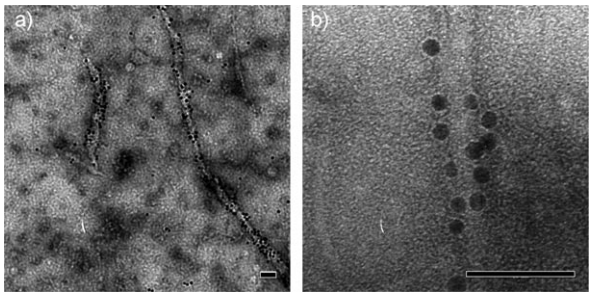

Figure 4. a) TEM micrograph of hPFO hybridized with Au–cDNA. b) Higher magnification image of the same system. TEM grids are stained with uranyl acetate. Scale bars are 50 nm.

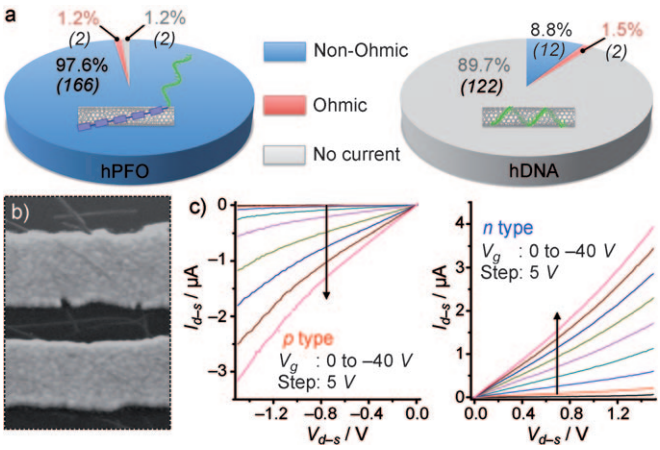

Figure 5. FET device fabrication with hPFO. a) Comparison of fabrication efficiencies, 99% and 10% bridging in total, for hPFO (left) and hDNA (right) devices, respectively. Numbers in parentheses denote the number of devices that exhibit the corresponding electrical behavior. b) SEM image of a sample bridging region from a hPFO device. c) FET characteristics for a representative hPFO device showing ambipolarity. Output curves in p- and n-type ranges (left and right, respectively). See Figure S26 for the transfer curves of the same device.

small degree of nanotube deposition through unspecific interactions is evidently unavoidable, the consistently higher coverage throughout the cDNA surface is a clear indication of successful immobilization through sequence-specific hybridization. The presence of SWNTs on the surface was also confirmed by Raman spectroscopy (Figure S24).

As an extension of this concept, we took advantage of the enriched semiconducting SWNT population of hPFO and our straightforward solution-processing paradigm to fabricate functional electronic devices. A mixed monolayer of complementary thiol–ODN and mercaptohexanol (MCH) was formed on lithographically defined electrodes (Figure S25, see the Supporting Information for details).[25] The final preparation of functional devices was then a simple matter of depositing a drop of hPFO solution on the substrate, repeatedly rinsing, and subsequently drying under N_2. Electrical contact was established in surprisingly high yield through the bridging of SWNTs between two electrodes upon DNA hybridization (Figure 1 d)—99% of the 170 thus fabricated devices carried current by bridging electrodes (Figure 5 a, left), as compared to only 10% of the 136 devices fabricated from hDNA, which does not contain addressable ss DNA (Figure 5 a, right). Remarkably, 98% of all hPFO devices showed non-Ohmic behavior; they were classified as functioning devices. It should be noted that the number of Ohmic circuits is always a subset of bridged electrodes. Our device fabrication yielded 10% higher bridging (99% vs. 90%) than a large-area method using dielectrophoretic deposition[26] with merely 1.2% of metallic SWNT bridging (Figure 5 f, left). However, in this example, the ratio of functional devices was not reported. In another comparable self-assembled system, the reported efficiency of functioning devices using covalently bonded DNA–SWNTs was only 10% (albeit with a wider channel) with no particular selectivity for semiconducting or metallic species.[27] Analysis of our *I*–*V* curves suggests that, as in the devices fabricated by Hazani et al.,[13c] conductivity in our devices may be governed by strong Schottky barriers at the contacts and junctions between SWNTs within the gap. SEM images of the hPFO and hDNA devices (Figure 5 b, S28 and S29) clearly revealed differences in the density of electrode-bridging immobilized SWNTs, which is in agreement with conductance measurements.

Out of the 168 functioning hPFO devices, less than 1.2% showed metallic behavior, far less than expected on the basis of the absorption spectra. Considering the geometry of our devices (inter-electrode gap: 240–360 nm, overlap region: 15 µm, Figure S25a–b) and the rarity of short circuits, our approach results in an extremely low population of addressable metallic SWNTs. A possible explanation for this result may be that the vast majority of metallic species observed in the UV/Vis spectra (< 600 nm absorption in Figure 2 a, Table S2) are dispersed by the wrapping of both the DNA block and the PFO segment, thus leaving such nanotubes unavailable for immobilization by Watson–Crick base pairing. Device fabrication using DNA hybridization would then represent an additional level of selectivity by removing imperfectly dispersed metallic SWNTs simply by rinsing away unhybridized material. A subset of 25 non-Ohmic hPFO devices was further investigated for FET behavior by using the bottom-gate electrode in vacuum. Remarkably, in light of the relatively crude aqueous device preparation and extended exposure to air, 80% of the devices worked as ambipolar FETs, with on/off ratios of up to 5×10^4 (Figure 5 c, S26 and S27).[28] Investigations are currently underway to determine whether the ambipolarity is related to the dense wrapping of the PFO layer or mediated by the SWNT–Au contact established by the MCH/DNA mixed monolayer.[29]

In conclusion, we have demonstrated a new concept for carbon-nanotube manipulation based on a hybrid material and offering an unprecedented degree of control over nanotube functionalization and assembly. This versatile system combines the advantages of polymers, such as the capability to selectively disperse semiconducting SWNT species, with the high degree of structural control inherent to DNA nanotechnology through solid-phase synthesis and self-recognition properties. The DBC is generated in a single synthetic process, and the hydrophobic polymer block is able to selectively disperse carbon nanotubes in water. This approach represents, to the best of our knowledge, one of the most selective aqueous carbon nanotube dispersions attain-

able, notably without additional purification steps. This result is already remarkable for stabilizing a range of semiconducting nanotubes for aqueous processing in a nondestructive manner, but the main impact of this work stems from the accessibility of the DNA block, which is not involved in the selective dispersion, for further manipulation. As we demonstrated with the use of gold nanoparticles, it is a simple matter to functionalize our nanotube dispersion by predictable and controlled Watson–Crick base pairing.

While dispersions with PFO and DNA alone do not present the opportunity for further versatile self-assembly, the entire DNA sequence is available for spatial adressability, thus leading to better defined and stronger base-pairing interactions. This approach offers the possibility to integrate the SWNT dispersions into protocols that allow the functionalization and manipulation of DNA on surfaces. Likewise, the dispersion of SWNTs with our DBC material allows the easy fabrication of operating SWNT-FETs in high yield, completely based on self assembly. Even without optimization of the contacts, SWNT alignment, or dielectrics, many of our transistors achieved a performance level comparable to reported single-SWNT-type devices with ambipolar conduction. The simple and efficient solution processing also makes it the only technique for single-SWNT-type device fabrication that easily could be adapted to large-scale production. Further investigations should focus on other practical uses of the DNA in combination with different polymers, for instance in nanotube-based biosensors and targeted therapeutics.[30]

Received: November 11, 2010
Published online: March 1, 2011

Keywords: amphiphiles · DNA · field-effect transistors · gold nanoparticles · nanotubes

[1] M. Hersam, *Nat. Nanotechnol.* **2008**, *3*, 387.
[2] a) D. Tasis, N. Tagmatarchis, A. Bianco, M. Prato, *Chem. Rev.* **2006**, *106*, 1105; b) M. Tchoul, W. Ford, G. Lolli, D. Resasco, S. Arepalli, *Chem. Mater.* **2007**, *19*, 5765.
[3] a) M. O'connell, S. Bachilo, C. Huffman, V. Moore, M. Strano, E. Haroz, K. Rialon, P. Boul, W. Noon, C. Kittrell, J. Ma, R. Hauge, R. Weisman, R. Smalley, *Science* **2002**, *297*, 593; b) V. Moore, M. Strano, E. Haroz, R. Hauge, R. Smalley, J. Schmidt, Y. Talmon, *Nano Lett.* **2003**, *3*, 1379; c) J. Amiran, V. Nicolosi, S. Bergin, U. Khan, P. Lyons, J. Coleman, *J. Phys. Chem. C* **2008**, *112*, 3519; d) C. Ehli, C. Oelsner, D. M. Guldi, A. Mateo-Alonso, M. Prato, C. Schmidt, C. Backes, F. Hauke, A. Hirsch, *Nat. Chem.* **2009**, *1*, 243.
[4] M. S. Arnold, A. A. Green, J. F. Hulvat, S. I. Stupp, M. C. Hersam, *Nat. Nanotechnol.* **2006**, *1*, 60.
[5] a) A. Nish, J. Hwang, J. Doig, R. Nicholas, *Nat. Nanotechnol.* **2007**, *2*, 640; b) J. Gao, M. A. Loi, *Eur. Phys. J. B* **2010**, *75*, 121.
[6] a) S. Tans, A. Verschueren, C. Dekker, *Nature* **1998**, *393*, 49; b) R. Martel, T. Schmidt, H. Shea, T. Hertel, P. Avouris, *Appl. Phys. Lett.* **1998**, *73*, 2447.
[7] P. Avouris, Z. Chen, V. Perebeinos, *Nat. Nanotechnol.* **2007**, *2*, 605.
[8] a) J. Misewich, R. Martel, P. Avouris, J. Tsang, S. Heinze, J. Tersoff, *Science* **2003**, *300*, 783; b) Y. Yao, X. Dai, C. Feng, J. Zhang, X. Liang, L. Ding, W. Choi, J.-Y. Choi, J. M. Kim, Z. Liu, *Adv. Mater.* **2009**, *21*, 4158.
[9] International roadmap committee, "International Technology Roadmap for Semiconductors" can be found under http://www.itrs.net **2009**.
[10] a) N. C. Seeman, *Nature* **2003**, *421*, 427; b) P. W. K. Rothemund, *Nature* **2006**, *440*, 297; c) J. Sharma, R. Chhabra, A. Cheng, J. Brownell, Y. Liu, H. Yan, *Science* **2009**, *323*, 112.
[11] a) M. Zheng, A. Jagota, E. Semke, B. Diner, R. Mclean, S. Lustig, R. Richardson, N. Tassi, *Nat. Mater.* **2003**, *2*, 338; b) X. Tu, S. Manohar, A. Jagota, M. Zheng, *Nature* **2009**, *460*, 250.
[12] S. Jung, M. Cha, J. Park, N. Jeong, G. Kim, C. Park, J. Ihm, J. Lee, *J. Am. Chem. Soc.* **2010**, *132*, 10964.
[13] a) W. Yang, M. J. Moghaddam, S. Taylor, B. Bojarski, L. Wieczorek, J. Herrmann, M. J. McCall, *Chem. Phys. Lett.* **2007**, *443*, 169; b) K. Keren, R. Berman, E. Buchstab, U. Sivan, E. Braun, *Science* **2003**, *302*, 1380; c) M. Hazani, D. Shvarts, D. Peled, V. Sidorov, R. Naaman, *Faraday Discuss.* **2006**, *131*, 325.
[14] a) J. F. Campbell, I. Tessmer, H. H. Thorp, D. A. Erie, *J. Am. Chem. Soc.* **2008**, *130*, 10648; b) Z. Zhou, H. Kang, M. L. Clarke, S. H. D. P. Lacerda, M. Zhao, J. A. Fagan, A. Shapiro, T. Nguyen, J. Hwang, *Small* **2009**, *5*, 2149.
[15] a) Y. Chen, H. Liu, T. Ye, J. Kim, C. Mao, *J. Am. Chem. Soc.* **2007**, *129*, 8696; b) H. T. Maune, S.-p. Han, R. D. Barish, M. Bockrath, W. A. Goddard, P. W. K. Rothemund, E. Winfree, *Nat. Nanotechnol.* **2010**, *5*, 61; c) K. Müller, S. Malik, C. Richert, *ACS Nano* **2010**, *4*, 649.
[16] a) M. Kwak, A. J. Musser, J. Lee, A. Herrmann, *Chem. Commun.* **2010**, *46*, 4935; b) M. Kwak, I. Minten, D.- M. Anaya, A. Musser, M. Brasch, R. Nolte, K. Müllen, J. Cornelissen, A. Herrmann, *J. Am. Chem. Soc.* **2010**, *132*, 7834.
[17] F. E. Alemdaroglu, N. C. Alemdaroglu, P. Langguth, A. Herrmann, *Adv. Mater.* **2008**, *20*, 899.
[18] D. Marsitzky, M. Klapper, K. Müllen, *Macromolecules* **1999**, *32*, 8685.
[19] F. Alemdaroglu, K. Ding, R. Berger, A. Herrmann, *Angew. Chem.* **2006**, *118*, 4313; *Angew. Chem. Int. Ed.* **2006**, *45*, 4206.
[20] Y. Tan, D. Resasco, *J. Phys. Chem. B* **2005**, *109*, 14454.
[21] H. Kataura, Y. Kumazawa, Y. Maniwa, I. Umezu, S. Suzuki, Y. Ohtsuka, Y. Achiba, *Synth. Met.* **1999**, *103*, 2555.
[22] Y. Ishibashi, T. Kobayashi, A. D. Prins, J. Nakahara, M. A. Lourenco, R. M. Gwilliam, K. P. Homewood, *Phys. Status Solidi B* **2007**, *244*, 402.
[23] J. Hwang, A. Nish, J. Doig, S. Douven, C. Chen, L. Chen, R. Nicholas, *J. Am. Chem. Soc.* **2008**, *130*, 3543.
[24] S. A. Claridge, H. W. Liang, S. R. Basu, J. M. J. Frechet, A. P. Alivisatos, *Nano Lett.* **2008**, *8*, 1202.
[25] T. Herne, M. Tarlov, *J. Am. Chem. Soc.* **1997**, *119*, 8916.
[26] A. Vijayaraghavan, S. Blatt, D. Weissenberger, M. Oron-Carl, F. Hennrich, D. Gerthsen, H. Hahn, R. Krupke, *Nano Lett.* **2007**, *7*, 1556.
[27] M. Hazani, D. Shvarts, D. Peled, V. Sidorov, R. Naaman, *Appl. Phys. Lett.* **2004**, *85*, 5025.
[28] P. Avouris, R. Martel, *MRS Bull.* **2010**, *35*, 306.
[29] a) X. Cui, M. Freitag, R. Martel, L. Brus, P. Avouris, *Nano Lett.* **2003**, *3*, 783; b) P. Collins, K. Bradley, M. Ishigami, A. Zettl, *Science* **2000**, *287*, 1801.
[30] a) M. T. Martinez, Y. C. Tseng, N. Ormategui, I. Loinaz, R. Eritja, J. Bokor, *Nano Lett.* **2009**, *9*, 530; b) K. Welsher, Z. Liu, S. P. Sherlock, J. T. Robinson, Z. Chen, D. Daranciang, H. Dai, *Nat. Nanotechnol.* **2009**, *4*, 773; c) D. A. Giljohann, D. S. Seferos, W. L. Daniel, M. D. Massich, P. C. Patel, C. A. Mirkin, *Angew. Chem.* **2010**, *122*, 3352; *Angew. Chem. Int. Ed.* **2010**, *49*, 3280.

